JOURNAL OF MATERIALS SCIENCE 39 (2004) 2747–2754

Pitting corrosion behavior of lead in Na_2HPO_4–$NaNO_3$ solutions

M. M. EL-NAGGAR
Chemistry Department, Faculty of Science, Benha University, Benha, Egypt

The pitting corrosion behavior of lead in 0.10 M Na_2HPO_4 solutions containing various concentrations from $NaNO_3$ has been studied using potentiodynamic anodic polarization and SEM techniques and complemented by both X-ray and FT-IR surface analysis. Above certain critical $NaNO_3$ concentration, the aggressive anions prevented the oxygen evolution and induce pitting on the Pb electrode surface. Pitting-initiation and pitting-growth were found to depend on the concentration of the aggressive NO_3^- anions. Also, some changes in the (I–E) curves within the active, pre-passive and passive regions were recorded. These changes imply mainly the appearance of new stages and peaks. This behavior gives an indication for definite changes in the pit-characteristics, which interpreted in terms of solution composition and kinetics of its associated processes within pits.

1. Introduction

Pitting is a form of extremely localized and intensive attack that results in a cavity or a hole in the metal. It is one of the most destructive forms of corrosion. In addition, pits tend to undermine or undercut the surface as they grow. Pitting corrosion of a metal could be initiated on a surface covered with a passive layer [1] and can occur only in solution containing an aggressive anion such as Cl^-, I^- and Br^- [1, 2] or NO_3^- [3]. An important feature of pitting-corrosion is that the attacks, which start at sensitive spots on the surface, sometimes spread out, sometimes may cease and heal to develop the weak points in the film and sometimes it remains localized producing intense attack or pitting.

The passivation behavior of lead in various alkaline solutions has been the subject of many investigations [4–12]. It has been reported that passivity of lead in alkaline solutions is due to the formation of PbO thick film on the lead electrode surface [10–12]. Also, in a previous publication by the present author [13], the electrochemical behavior of lead electrode in 0.10 M Na_2HPO_4 solutions was studied using cyclic voltammetric technique. It was clearly observed that several features characterize the forward anodic branch of the voltammogram namely: A, B, C, D and E, which are represented schematically in Fig. 1. It was also concluded that peak A corresponds to the oxidation of Pb to $Pb(OH)_2$ and/or PbO (depending on the scan rate). Peak B corresponds to 2-D nucleation of PbO and could be capable of spreading over the surface and throwing the remaining $Pb(OH)_2$ out in solution and the passive—span (plateau C) was related to the 3-D nucleation and thickening of the passive (PbO) surface film. Moreover, the two regions D and E were attributed to the electroformation of PbO_2 and the oxygen evolution, respectively. Comparatively, very little work has been published on the passivity-breakdown and on the initiation of pitting corrosion of lead in the near alkaline solutions.

The objective of the present work is to study the potentiodynamic anodic polarization behavior of lead in the slightly alkaline 0.10 M Na_2HPO_4 solutions containing various concentrations from the $NaNO_3$ aggressive agent. Particular attention has been given to the main characteristics of the pitting phenomena such as passivity breakdown, pit-initiation, pit-growth and pit-propagation conditions, its critical potentials and its critical concentrations as well as to gain more knowledge on the nature of pits and to get deeper insight on the conditions allowing various stages of pitting corrosion to takes place.

2. Experimental

The chemicals were analytical grade reagents (Merck) and used without further purification. Solutions are prepared using doubly distilled water.

A cylindrical lead electrode was used in experiments, with 0.385 cm^2 cross-sectional area, directly made from 99.99% pure lead rods (Aldrich). It was embedded in the epoxy resin mold and only its cross-section was allowed to contact the electrolyte. Prior to each experiment, the electrode surface was polished with successively finer grades of emery paper, then degreased with acetone, washed with running doubly distilled water, and finally dried with filter paper.

A conventional electrolytic cell was used with a saturated calomel electrode (inside a luggin's capillary probe) as reference electrode and a platinum foil (separated from the cell solution by a sintered glass frit) as counter electrode. The surface of the working electrode was always kept in close touch with the luggin capillary

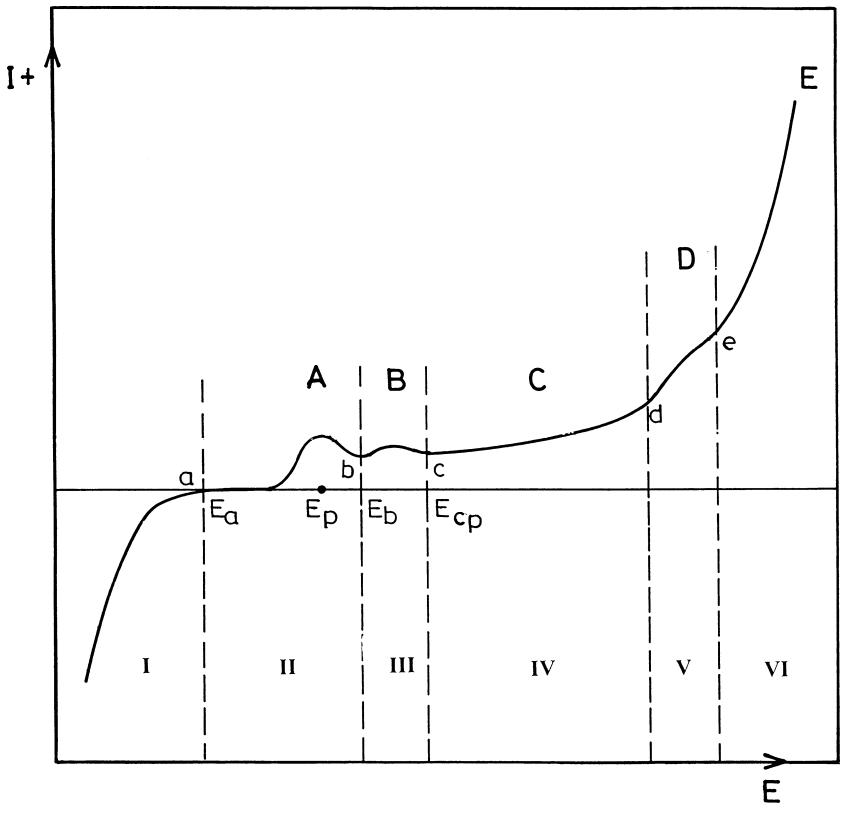

Figure 1 Schematic presentation of the forward cyclic voltammogram curve of Pb electrode in 0.10 M Na_2HPO_4 solution between the hydrogen and oxygen evolution of the metal (I) hydrogen evolution; (II) active region; (III) pre-passive region; (IV) passive region; (V) trans-passive region; and (VI) oxygen evolutoin.

tip to minimize the IR drop through the cell. Potentiodynamic anodic polarization studies were carried out using a wenking potentioscan (type pos. 73). The anodic polarization curves were recorded from −1.8 to +0.2 V and plotted using X-Y recorder (Cole Parmer Instruments, USA) at a scan rate of 25 mV/sec. All the experiments were conducted at room temperature (25 ± 1°C).

Scanning electron microscopy (SEM) tests were made on the electrode surface after potentiodynamically anodic polarization experiments at a scan rate of 25 mV/sec in 0.10 M Na_2HPO_4, free or containing some selected concentrations from $NaNO_3$. SEM examinations were made with a Joel Model JSM 50.

Also, the salt that formed on the lead electrode surface was collected after the experiments and analyzed using X-ray diffraction and FT-IR spectroscopic methods.

3. Results and discussion

3.1. The potentiodynamic anodic polarization measurements

The results of the present study on the potentiodynamic anodic polarization measurements for lead anode in 0.10 M Na_2HPO_4 solutions in the absence and in the presence of various concentration of the aggressive NO_3^- anion (0.01–0.20 M) are shown plotted in Fig. 2 (curves 1–14). It can be clearly seen that these curves manifests a number of interesting features, which are summarized in Table I.

In the 0.10 M Na_2HPO_4 free-$NaNO_3$ solution (curve 1, Fig. 2), the present poteniodynamic anodic polarization curve is identically the same as that of the forward branch of the previously studied cyclic voltammogram [13]. Accordingly, the characteristic features of curve 1 of the present anodic polarization curves are the same as that mentioned in the introduction and is schematically shown in Fig. 1.

Critical inspection of curves (1–14) shown in Fig. 2 reveals that, in presence of different $NaNO_3$ concentration, the rates of lead oxidation are significantly greater than those measured in 0.10 M Na_2HPO_4 solution and it appears to be four ranges of $NaNO_3$ concentration, in which the anodic behavior changes. Thus, depending on the range of $NaNO_3$ concentration, there are four different distinct groups of behaviors namely:

a. Group I, Low concentration range (≤0.03 M $NaNO_3$), curves 1–5.

b. Group II, Intermediate concentration range (0.04–0.06 M $NaNO_3$), curves 6 and 7.

c. Group III, High concentration range (0.12–0.18 M $NaNO_3$), curves 8–11.

d. Group IV, Limiting concentration range (0.185–0.200 M $NaNO_3$), curves 12–14.

To give an insight into the anodic polarization behavior of lead in 0.10 M Na_2HPO_4 containing various concentrations from NO_3^- anion and for the sake of simplicity, results of each of the above mentioned four distinct groups will be described and interpreted separately.

3.1.1. Group I

Within this range of $NaNO_3$ concentration, the anodic polarization curve 2 of Fig. 2 is practically coinciding

TABLE I Effect of presence of increasing concentrations of $NaNO_3$ on the potentiodynamic anodic polarization characteristics of lead electrode in 0.10 M Na_2HPO_4 solution (see Fig. 2)

Curve number (Fig. 2)	NO_3^- concentration (M)	Characteristic features	
		Active region	Passive and transpassive region
1, 2	0.00, 0.01	a, A, b	B, C, D and oxygen evolution
3–5	0.02–0.03	a, A, b	B, C
6, 7	0.04, 0.06	a, A, b	Two arrests (I and J), pit initiation
8	0.12	a, A, b	One peak (L)
9–11	0.14–0.18	a, A, b	Two peaks (M and N), different types of pits
12–14	0.185–0.200	a, A, b	Sudden increase in current density

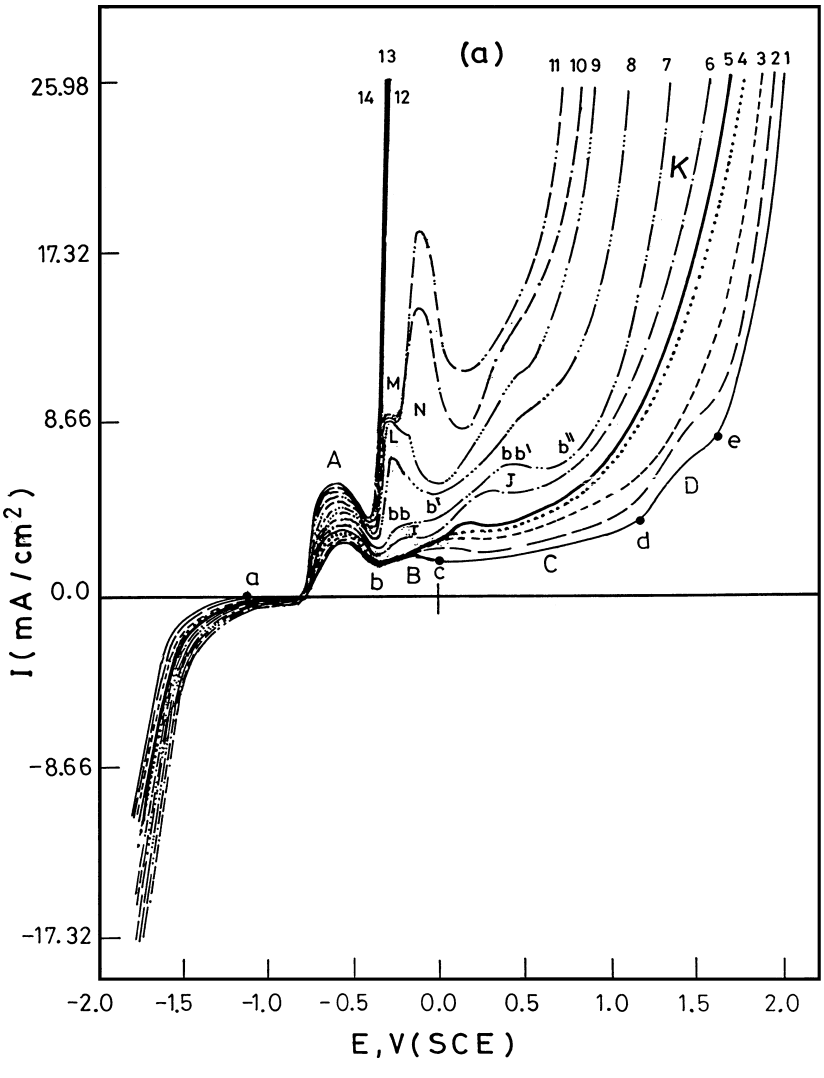

Figure 2 Potentiodynamic anodic polarization curves of Pb in (a) 0.01 M Na_2HPO_4 solutions containing different concentration from $NaNO_3$ at voltage scan rate of 25 mV/sec (1) free $NaNO_3$; (2) 0.01 M; (3) 0.02 M; (4) 0.025 M; (5) 0.03 M; (6) 0.04 M; (7) 0.06 M; (8) 0.12 M; (9) 0.14 M; (10) 0.16 M; (11) 1.08 M; (12) 0.185 M; (13) 0.19 M; and (14) 0.20 M.

with that of the basic supporting electrolyte (curve 1). Further increase in the NO_3^- anion content within this low concentration range (curves 3–5, Fig. 2), leads to some minor changes. Apparently, the shoulder D in the transpassive region starts to disappear, the passive span C starts to shorten and the potential of the final unlimited current rise shifts to less positive values. Also, it is quite clear that, there is a slight increase in the current density over the entire polarization curves. Moreover, a slight shift in the potential of peak A towards more negative values and that of peak B towards to more positive values is observed. Furthermore, no indication for pitting corrosion is observed.

This would indicate that NO_3^- anions have a stimulating effect on the active dissolution of lead, which could be related to the competitive adsorption between the NO_3^- and the OH^- anions for adsorption sites on the electrode surface. The adsorbed NO_3^- anions may accelerate the active dissolution of lead through a direct participation in the elementary act of the ionization of lead. However, the shift of peak B potentials to more positive values could be attributed to film repair and healing.

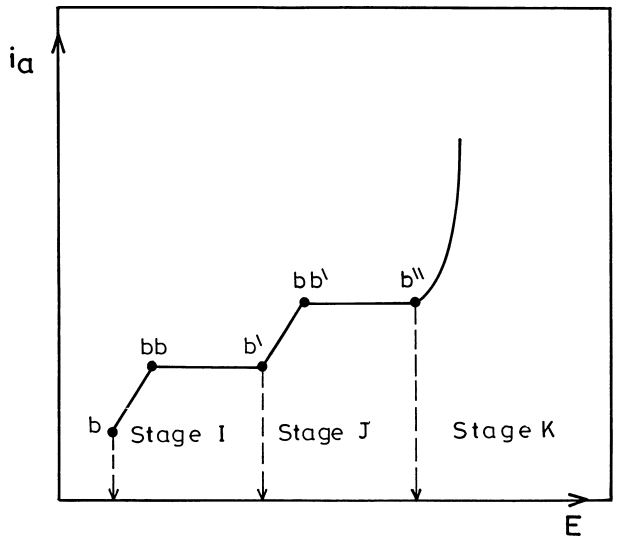

Figure 3 Schematic representation of the tripartition potentiodynamic anodic polarization curve characterizing the dependence of rate of anodic dissolution (current density; i_a) on the potential E.

Apart from these minor changes, this low concentration $NaNO_3$ range did not change the shape of the polarization curves indicating that the nature of the passivating film remains the same.

3.1.2. Group II

In this range of $NaNO_3$ concentration, the potniodynamic anodic polarization curves 6 and 7 of Fig. 2 are characterized by the consecutive stages (I, J and K). Each of stages (I and J) consists of two well defined consecutive steps namely: an initial rise in current followed by a definite arrest along which the current is independent on potential. Finally, at the end of stage J the current is suddenly rises during stage K to the final unlimited value. Moreover, it appears that the three initial potentials at points b, b\ and b\\ of the three stages (I, J and K) are considered as a critical potentials (for more illustration see Fig. 3 and Table II).

Also, it is observed that this range of NO_3^- anion concentration obliterates oxygen evolution and causes the appearance of a very limited number of insoluble white spots on the electrode surface during the final, unlimited current rise along stage K. The composition of the white spots was identified as $Pb_5(PO_4)_3OH$ (see below).

In order to give more knowledge on the two stages (I and J) of curves 6 and 7, a separate experiment was carried out in presence of 0.04 M $NaNO_3$ as an attempt to produce its reduction branch. It is illustrated from Fig. 4 that on reversing the direction of potential at +1.25 V no reduction branch was observed but irregular oscillations started and remained without any reversing. This behavior would indicate that the lead electrode enters into an unstable state, in which it started to be activated and passivated.

As supporting evidence to the above-mentioned discussion, SEM was cared out on the lead electrode surface at the end of experiment of curve 6. It revealed the occurrence of pitting corrosion (see Fig. 5b).

On the basis of the results described above it could concluded that the appearance of the two stages I and J would be most probably attributed to two main consecutive stages of the pitting corrosion corresponding to breakdown of passive film stage (I) followed by pit-nucleation stage (J).

During stage I, the adsorbed NO_3^- anion starts to penetrate the oxide film under the influence of a high electric field at potential of point b (the onset of stage I). The penetration of the aggressive anion can be expected to create an equal but opposite charges on the metal side of the oxide film. When this ultimately reaches a critical density, a breakdown through the oxide film takes place at some location, while the major part of the metal surface remains passive. The penetration and consequently the breakdown of the passive film are dependent on the rate of ion transportation through the oxide film, the thickness of the film, the ion selectivity of the film and the potential. Moreover, the appearance of the current arrest of stage I could be account for the presence of a dynamic equilibrium between the healing of the locations at which the breakdown of the oxide film takes place and the breaking of newly ones.

When the potential becomes sufficiently positive at point b\ (the onset of the second stage J), localize attack forming pit nuclear is assumed to start. Thus, point b\ potential could be considered the critical potential for pit-nucleation. Moreover, the appearance of the current arrest of stage J could be account for the presence of a dynamic equilibrium between passivatable pits and newly evolving ones.

The rise in current density of curves 6 and 7 at the end of stage J (point b\\), could be attributed to the beginning of a new stage (K) namely pit-growth process. Thus, the potential of point b\\ is the critical potential for the pit-growth of a limited number of pits that are assumed to initiate during stage J while the major part of the metal surface remains passive. Thus, during pit-initiation stage, anodic spots are surrounded by cathodic area were created. In this case, attack while starts at sensitive spots continue to remain localized

TABLE II The critical potentials and current densities of the characterized points of stages (I and J) of the pit-initiation stages of curves 6 and 7—Fig. 2

NO_3^- concentration (M)	The potential and current density at points b, bb, b\, bb\ and b\\ (Fig. 3)									
	b		bb		b\		bb\		b\\	
	E (V)	i (mA/cm^2)	E (V)	i (mA/cm^2)	E (V)	i (mA/cm^2)	E (V)	i (mA/cm^2)	E (V)	i (mA/cm^2)
0.04	−0.375	1.65	−0.250	2.98	−0.060	2.98	0.270	5.68	0.570	5.68
0.06	−0.375	1.70	−0.220	3.79	0.000	3.79	0.375	6.5	0.690	6.5

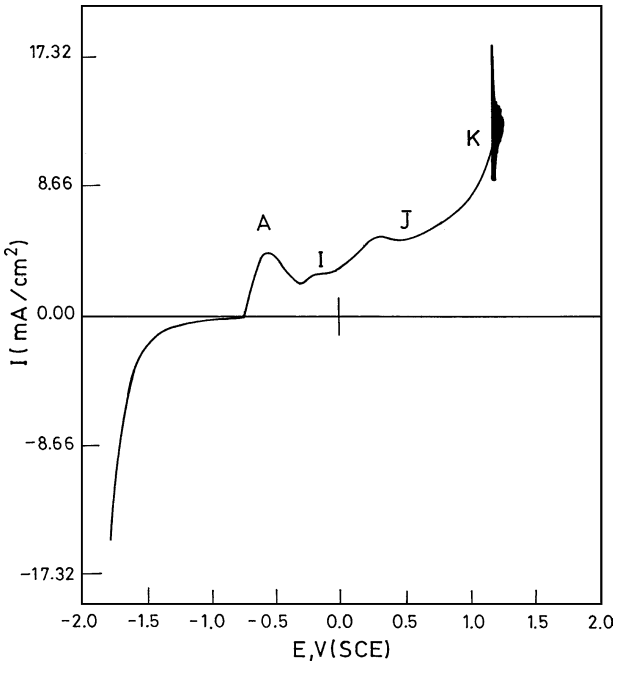

Figure 4 Effects of anodic reversal potential on Pb electrode in 0.10 M Na_2HPO_4 containing 0.04 M $NaNO_3$ solution at voltage scan rate of 25 mV/sec.

producing pit growth. Therefore, the current density on the anodic spots is so high that a deep pit is formed leading to the destruction of the metal. As the result, the corrosive-pit will protect cathodically the adjacent area from corrosion. Since the solubility in pits is limited, an extensive accumulation of the metal ions within pits will move outward and react with phosphate anions forming a white spots ($Pb_5(PO_4)_3OH$) that precipitate out onto the pits. In conclusion, pit-growth in area occurs during the stage K, while the major part of the surface area remains passive.

It is of interest to remark from Fig. 2 (curves 6 and 7) and Table II that, the two critical potentials (b$^{\backslash}$ and b$^{\backslash\backslash}$)) are found to shift toward more positive values as the aggressive NO_3^- anion concentration increases. In view of the well-established rule aggressiveness of NO_3^- anions, this appears somewhat unusual. The difficulty disappears however, when the complimentary cathodic reaction is taken into consideration. Under the present experimental condition, oxygen reduction is by far the major cathodic process contributing to corrosion. As the result of high alkalinity resulting from the cathodic reaction attack on the oxide will take place exposing momentarily the bare metal surface. Thus, the system appears to be under cathodic control. For it that pitting corrosion occurs despite the ennobling in potential indicative that attack is cathodically contributed.

Furthermore, it is illustrated from curves 6 and 7 of Fig. 2 that the sudden rise in current density at point b$^{\backslash\backslash}$ is assumed to be the limiting stage (K) in the dissolution process. There is reason to believe that the theory of retarded discharge can be used to describe the anodic dissolution of the metal. Consequently, if ionization of the metal is assumed to be the limiting stage in the dissolution process, then the rate of the anodic process (i_a) must be exponential factor of the potential according to the following relation [14]:

$$i_a = \mathrm{K} \exp[(\alpha n \varphi_a F)/(RT)]$$

This equation shows that, the more the potential is shifted towards positive values, the higher will be the dissolution rate.

3.1.3. Group III

Within this range of $NaNO_3$ concentration, the potentiodynamic anodic polarization curves 8–11 of Fig. 2 are characterized by a high increase in the current density over the entire polarization curves as well as a number of interesting features, which are summarized in Table I. It is illustrated that the two arrests of the two stages (I and J) of curve 7 developed into unusual anodic peak L (curve 8) with peak potential of −0.250 V. Furthermore, the anodic peak L resolves into two unusual oxidation peaks (M and N) in curve 9. Peak N appears at more noble potential ($E_{\text{peak N}} = -0.190$ V) to that of peak M ($E_{\text{peak M}} = -0.300$ V), with peak current of M slightly higher than that of peak current N. On further increase of NO_3^- anion within this range of concentration (curves 10 and 11), the current density of peak N becomes much higher than that of peak M.

Also, it is observed that during the period of experiments within this $NaNO_3$ concentration range, a white solid deposit develops on the metal surface in the form of separated islands. These increase both in number and area as the potential moves in the positive direction. The white deposit does not adhere strongly to the metal surface and can be easily detached by rubbing with a moistened piece of filter paper. At their places the occurrence of uneven pit-attack can be seen on the metal surface.

In conclusion, within this high $NaNO_3$ concentration region, the appearance of one or two unusual anodic peak could be attributed to the presence of different types of pits.

Peak L (Fig. 2, curve 8) could be attributed to the development of pits, which most probably correlated to solution–composition within corrosive-pits. As the results of rapid dissolution within the pits, an excess of positive charges within the pits is expected resulting in the migration of more NO_3^-, OH^- and HPO_4^{2-} to maintain the electrical neutrality. As the result of hydrolysis, high acidic concentration occurs that stimulate dissolution of the metal and the entire process is accelerated. Thus, concentrations of various ionic species within pit (i.e., Pb^{2+}, H^+, HPO_4^{2-}, OH^- and aggressive NO_3^- anion) are different from that in the bulk electrolyte. Critical concentrations concept of the various contributions must be exceeded for stable pit growth to occur.

The two anodic peaks M and N (Fig. 2, curves 9–11) could be attributed to the presence of different types of pitting corrosion, which most probably correlated to the critical concentration of both the hydrogen and NO_3^- aggressive anions inside the pit. According to Sato's theory [15, 16], when the critical hydrogen ion concentration is reached, etching pit type is developed, whereas when the critical aggressive anion concentration

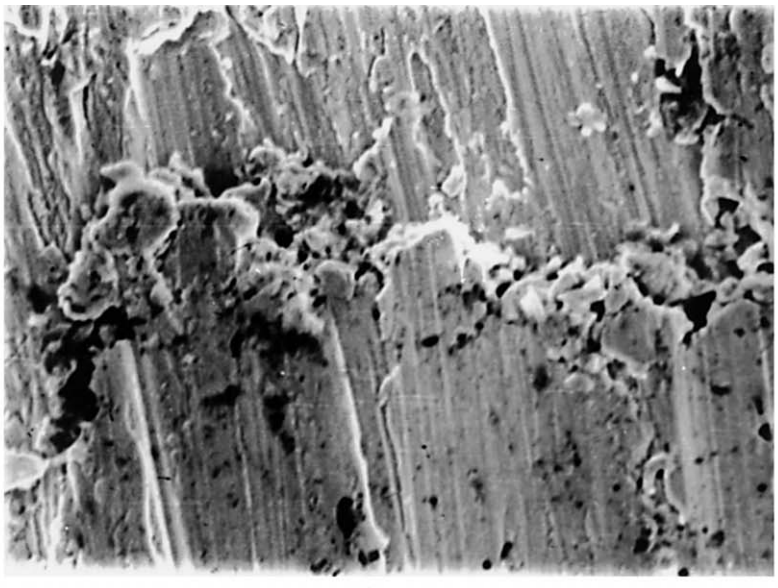

(a)

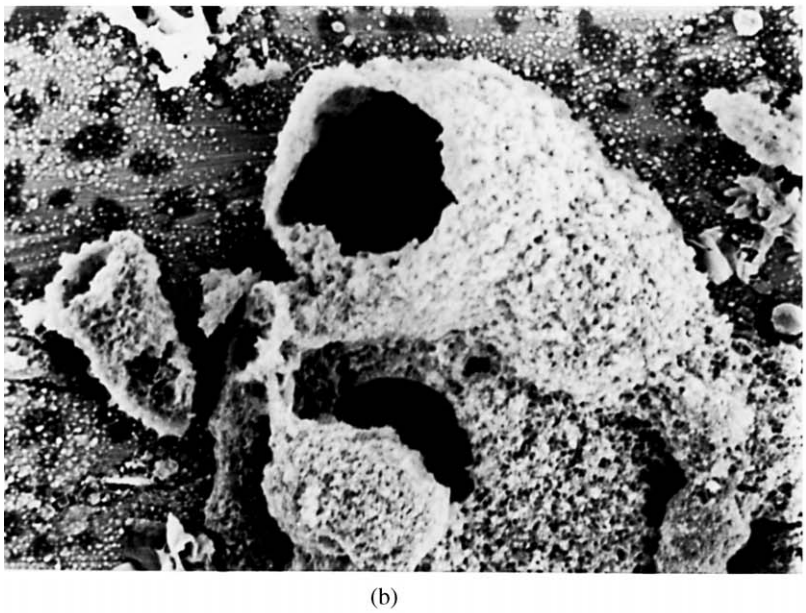

(b)

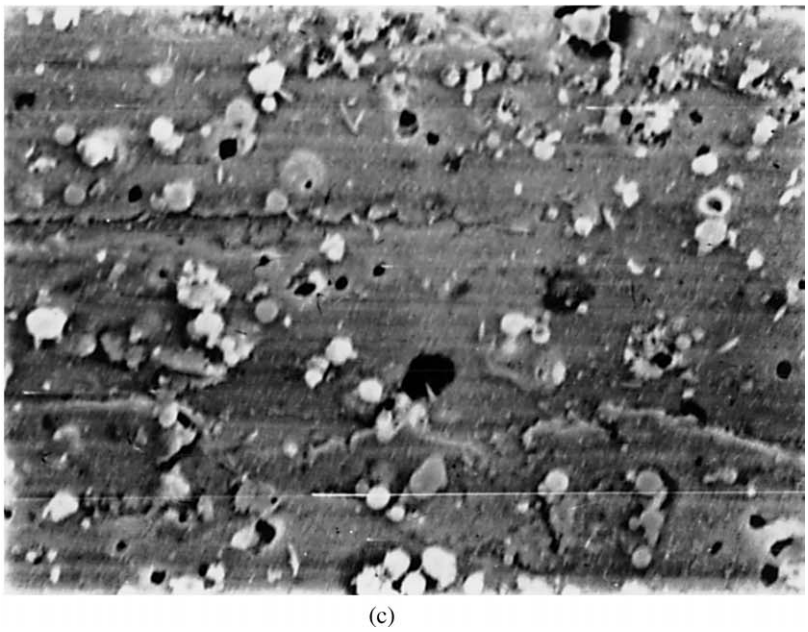

(c)

Figure 5 SEM—micrographs of Pb surface in 0.10 M Na_2HPO_4 solution containing different $NaNO_3$ concentrations: (a) free $NaNO_3$; (b) 0.04 M; and (c) 0.20 M.

is reached another pit type namely brightening pit is developed. Moreover, the developments of the etching pits occur at potential more active than the brightening pits. Since peak N is observed at more noble potential to that of peak M, thus it appears that etching pits is the most probable pit-type corresponding to peak M, whereas brightening pits is the most probable pit-type corresponding to peak N. On the other hand, peak L (Fig. 2, curve 8) would represent the boundary condition between peaks M and N.

3.1.4. Group IV

In this concentration range of $NaNO_3$, the potentiodynamic anodic polarization curves 12–14 of Fig. 2 show a sudden and sharp increase in the current density immediately after peak A at point b to unlimited value. Moreover, the curves 12–14 practically coincide forming one group of curves, which are well, separated from the other curves indicating a limiting condition.

Visual observations of the electrode surface during the experiments within this concentration range of $NaNO_3$ reveals the appearance of a white scatter particles on the electrode surface, which readily dissolve in the supporting electrolyte. Moreover, the presence of a huge number of uneven pit-attack on the metal surface can be seen after experiments.

It follows that pit-state formation could be developed within this group IV of $NaNO_3$ concentration. In this case, the localized corrosion is explained through the hindering of metal passivation due to local accumulation of the NO_3^- aggressive anions on the electrode surface, which favoring pit-state formation. It has been reported that [17, 18] a different electrode state (pitting-state) consisting of adsorption layer of thin poreless salt film, which prevent pre-passivation of the metal surface at a potential corresponding to the pitting potential. At this potential, layer grows in thickness and film becomes porous.

Also, the soluble white scattered particles, which is formed on the electrode surface during the final, unlimited increase in the current density could be due to the formation of a temporary soluble salt containing Pb^{2+} cation moving out from the pit interior.

3.2. Further tests

As supporting evidence to the above-mentioned discussion, the following extra experiments on both the electrode surface and the corrosion products formed were cared out using SEM, X-ray and FT-IR surface analysis techniques.

3.2.1. SEM examination of Pb surfaces

Fig. 5a, b, and c show three SEM images for lead electrode surface at the end of potentiodynamic anodic polarization experiments in 0.10 M Na_2HPO_4 solutions without and with certain concentrations from $NaNO_3$. In nitrate free solution, the SEM (Fig. 5a) showed the presence of a protective film, in which no evidence for the presence of pitting corrosion. In presence of 0.04 M $NaNO_3$, few numbers of pits containing white deposit are observed (Fig. 5b). In presence of 0.20 M $NaNO_3$ a large number of pits with the disappearance of the white deposit are shown (Fig. 5c).

3.2.2. X-ray and FT-IR surface analysis

The white spots formed on the lead electrode surface are collected at the end of potentiodynamic anodic polarization experiments in 0.10 M Na_2HPO_4 solution containing 0.04 M $NaNO_3$ and analyzed by using X-ray diffraction and IR-spectroscopy techniques. According to the results obtained from X-ray diffraction analysis (Fig. 6), the composition of the white spots is identified as $Pb_5(PO_4)_3OH$. The characteristics bands of Pb—O, PO_4, P═O and OH functional groups of $Pb_5(PO_4)_3OH$ compound (white spots) are also observed in the IR spectrum as shown from Fig. 7.

It must be emphasized that the reported X-ray spectrum is probably a mixture of PbO and /or a same high-oxidized state. So that the film will be referred to as

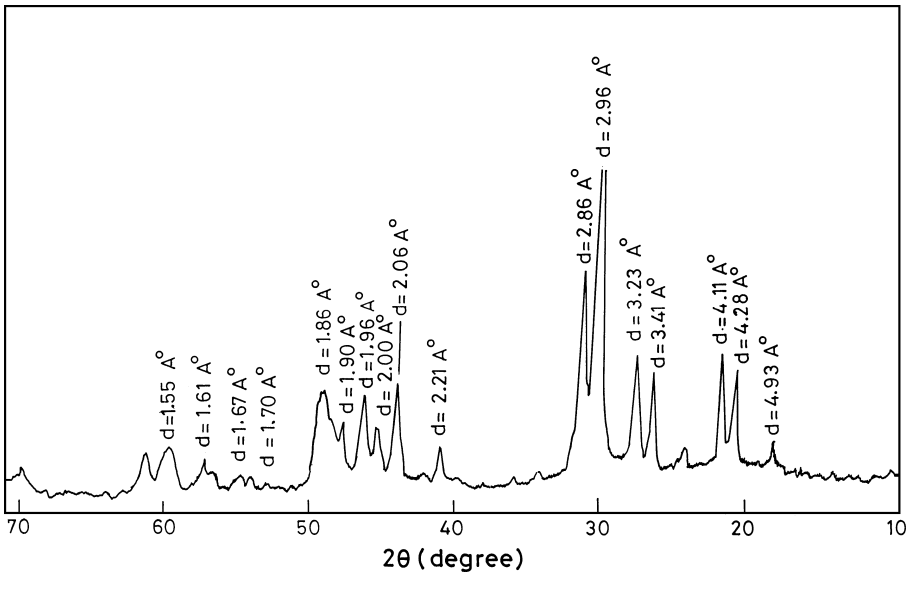

Figure 6 X-ray diffraction of the white precipitate formed on the Pb electrode surface.

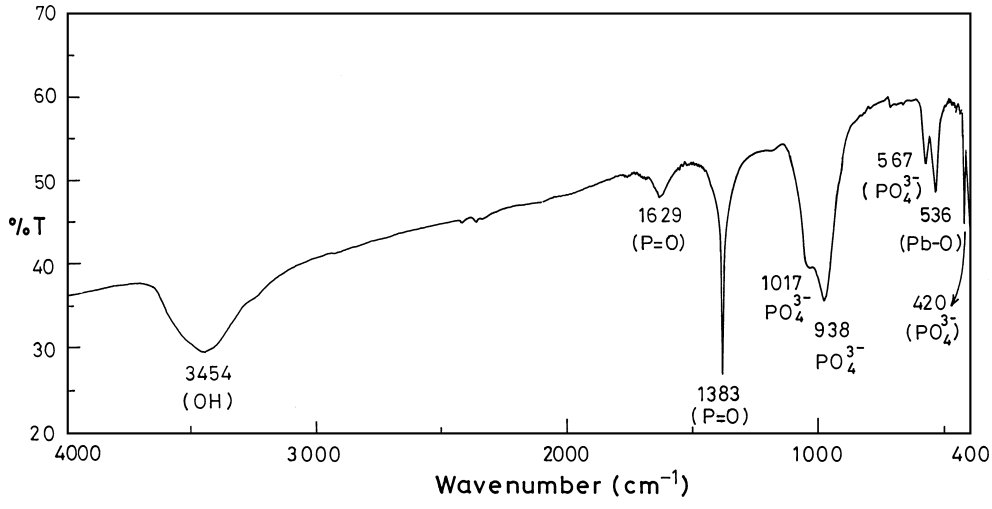

Figure 7 Infrared spectra of the white precipitate formed on the Pb electrode surface.

"mixed-valence" that constitutions of passive film consists of species that at best resemble oxides and high oxides of lead. However, this should not be misinterpreted to mean that the composition of the white spots are necessarily identical to the bulk crystalline super oxide as $Pb_5(PO_4)_3OH$.

4. Conclusions

Anodic potentiodynamic polarization and SEM experiments were carried out on Pb in 0.10 M Na_2HPO_4 solution in the absence and presence of $NaNO_3$ as pitting corrosion agent at a scan rate of 25 mV/sec. The results of these experiments revealed the following points:

1. In Na_2HPO_4 solution, difference between critical breakdown and localized attack stages under the prevailing conditions is sufficient to affect resolution.
2. A number of potentials characterizing the state of Pb electrode, the nature of the anodic process and its rates were evaluated.
3. The results demonstrated that, below a certain $NaNO_3$concentration ($\leq$0.03 M), the same form of the anodic polarization curves is recorded as obtained in case of blank solution. This behavior indicates that the NO_3^- anion does not interfere with the mechanism of passivation as far as oxide formation is concerned.
4. In presence of NO_3^- aggressive anion concentration in the range from 0.04 M to 0.06 M, the anodic polarization curves are characterized by three consecutive stages, which account for passivity breakdown, pit-initiation and pit-growth, respectively.
5. The shapes of the polarization curves are affected drastically and manifest a number of interesting features in presence of high concentration range (0.12–0.18 M) from $NaNO_3$, which are discussed.
6. Within $NaNO_3$ concentration range from 0.185 to 0.200 M, the results demonstrated the behavior of pitting-state formation.

References

1. YA. M. KOLOTYRKIN, *Corrosion* **19** (1963) 261.
2. Z. SZKLARSKA-SMIALOWSKA, *ibid.* **27** (1971) 223.
3. S. S. ABD EL REHIM and N. F. MOHAMED, *Corros. Sci.* **40** (1998) 1883.
4. M. FLEISCHMANN and H. R. THIRSK, *Trans. Faraday Soc.* **51** (1955) 71.
5. P. JONES, H. R. THIRSK and W. F. K. WYNNE-JONES, *ibid.* **52** (1956) 1003.
6. W. HOFFMAN, "Lead and Lead Alloys," 2nd ed. (Springer-Verlag, New York, 1970).
7. A. A. ABDUL AZIM and M. M. ANWAR, *Corros. Sci.* **9** (1969) 245.
8. A. A. ABDUL AZIM and K. M. EL-SOBKI, *ibid.* **12** (1972) 207.
9. L. M. PETER, *J. Electroanal. Chem. Interf. Electrochem.* **182** (1985) 333.
10. V. I. BIRSS and M. T. SHEVALIER, *J. Electrochem. Soc.* **134** (1987) 802.
11. *Idem.*, *ibid.* **134** (1987) 1594.
12. *Idem.*, *ibid.* **137** (1990) 2643.
13. M. M. EL-NAGGAR, Accepted for Publication (in press) in *J. Power Sources.*
14. I. L. ROZENFELD, "Corrosion Inhibitors" (McGraw-Hill Inc, New York, 1981) p. 6.
15. N. SATO, "Corrosion and Corrosion Protection," edited by R. P. Frankenthal and F. Mansfeld (The Electrochemical Society, Pennington, N. J., 1981) p. 101.
16. N. SATO, *J. Electrochem. Soc.* **129** (1982) 260.
17. H. H. STREHBLOW and J. WENNERS, *Electrochim. Acta* **22** (1977) 421.
18. H. BOHNI, "Corrosion Mechanisms," edited by F. Mansfeld (Marcel Dekker, Inc. New York, 1987) p. 250.

Received 13 May
and accepted 11 December 2003